Original research article

Measurement of the distribution of temperature and emissivity of a candle flame using hyperspectral imaging technique

Shu Zheng[a,*], Li Ni[a], Huawei Liu[a,*], Huaichun Zhou[b]

[a] Key Laboratory of Condition Monitoring and Control for Power Plant Equipment of Ministry of Education, School of Energy, Power and Mechanical Engineering, North China Electric Power University, Beijing 102206, China
[b] School of Energy and Power Engineering, Northeast Electric Power University, Jilin 132012, China

A B S T R A C T

A candle flame is experimentally studied using a hyperspectral imaging device in this paper. The distributions of temperature and wavelength-dependent emissivity are calculated using a Newton-type iterative method. The results show that the spectral radiation intensity increases from the outside to the inside in the candle flame, and at the same spatial point, the intensity increases as the wavelength increases. The highest temperature of the candle flame is about 1980 K, occurs close to the flame border, indicating the most vigorous reaction. Additionally, the radiation characteristics of the candle flame differ from a gray-body, and the emissivity of the flame decreases as the wavelength increases.

1. Introduction

A candle flame exemplifies the basic nature of a diffusion flame in the study of fire. It involves the evaporation of a liquid fuel from a porous surface, and unlike an uncontrolled fire, quickly reaches a steady state. Recently, research has been carried out on candle flames to study different applications and different conditions, including electric field effects [1], flame flickering [2], microgravity experiments [3,4], smoke point measurements [5], fire safety [6], flame shape analysis [7], and numerical models [8–11]. However, a systematic study on measurement of temperature and emissivity of candle flames has not been reported to date.

Arpit Patel [12] measured temperature of a candle flame using a CCD camera, the flame temperature is between 1450 K to 1700 K in this experiment. Thomsen [13] measured soot temperature in candle flames. He concluded the peak soot temperature remains between 2000 and 2200 K. The measured temperature of candle flame in the literatures are inconsistent. Many researchers have devoted their research work to temperature measurements in flames using nonintrusive optical techniques [14–16]. Tunable diode laser absorption spectroscopy [17–19], laser-induced incandescence [20], and emission-based tomography [21,22] all have proved to be reliable tools. De Iuliis et al. [23] and Snelling et al. [22] used a multiwavelength flame emission technique for high spatial resolution determination of soot temperature and soot volume fraction in axisymmetric laminar diffusion flames.

From the perspective of spectral resolution, the multi-wavelength method is a reliable measuring technique. Recently, the hyperspectral imaging device was developed. This technique measures the radiation intensity of a large number of continuous bands at each imaging unit by using hyperspectral imaging equipment, adding a spectral dimension to the traditional two spatial dimensions. High spectral imaging technology can provide measurement images containing spatial and spectral information [24,25]. For any material, the radiative reflection, absorption and emission energy varies with the change of wavelength, and the spectral information

contains the change trend, which is a direct reflection of the composition information of the material [26]. It has been successfully used in the agriculture, medicine, and safety applications [27], etc. The camera on the market either has high spatial resolution but low spectral resolution, or has high spectral resolution but low spatial resolution, but the hyperspctral imaging device has both high spatial resolution and high spectral resolution. The flame radiation intensity is determined by emissivity and blackbody radiation intensity, at the same time, the blackbody radiation intensity is determined by temperature. Therefore, the temperature and emissivity can be calculated from the flame radiation intensity. As far as we know there is no research investigating the candle flame using hyperspectral imaging technique.

In this paper, firstly, a Newton-type iterative method was proposed to solve the polynomial coefficients of radiative parameters and wavelength. Secondly, data processing and results from an experiment on a candle flame using the hyperspectral imaging technology will be presented and the corresponding discussion will be given. Additionally, some conclusions are provided.

2. Methodology

According to Wien's Law, radiation intensity can be expressed as [28]:

$$I(\lambda, T) = \varepsilon(\lambda){\cdot}I_b(\lambda, T) = \varepsilon(\lambda){\cdot}\frac{c_1}{\pi\lambda^5 e^{c_2/\lambda T}} \tag{1}$$

Where, $\varepsilon(\lambda)$ is the emissivity which is the function of the wavelength λ, c_1 and c_2 are constants, T is the temperature. The radiation intensity of the object under test is known, and the emissivity and temperature are the unknowns to be solved. Obviously, the number of unknowns is one more than that of known conditions, making the problem ill-posed and difficult to solve. To avoid this kind of ill-posed phenomenon mention above, a method is proposed to solve the relationship between emissivity and wavelength by reducing the number of unknown values.

According to the Taylor series, emissivity $\varepsilon(\lambda)$ can be expressed as a function of the wavelength λ [29]:

$$\varepsilon(\lambda) = a_0 + a_1{\cdot}\lambda + a_2{\cdot}\lambda^2 + ...a_n{\cdot}\lambda^n \tag{2}$$

where a_1, a_2, …, a_n are the polynomial coefficients, then Eq. (1) can be rewritten as:

$$I(\lambda, T) = (a_0 + a_1{\cdot}\lambda + a_2{\cdot}\lambda^2 + ...a_n{\cdot}\lambda^n){\cdot}\frac{c_1}{\pi\lambda^5 e^{c_2/\lambda T}} \tag{3}$$

So, the question becomes how to solve a_1, a_2, …, a_n and T with radiative intensities $I(\lambda_1)$, $I(\lambda_2)$, …, $I(\lambda_m)$.

The equations to be solved can be expressed as:

$$\alpha_j{\cdot}I(\lambda_j, T) - \alpha_j{\cdot}(a_0 + a_1\lambda_j + a_2\lambda_j^2 + ...a_n\lambda_j^n){\cdot}\frac{c_1}{\pi\lambda^5 e^{c_2/\lambda_j T}} = 0, j = 1, 2, ...,m. \tag{4}$$

Where, α_1, α_2, …, α_m are the weight coefficients. A Newton-type iterative method can be used to solve Eq. (4) in this paper.

The main process of the solution procedure can be seen in Fig. 1 and shown as follows.

1) Equation deviation

Eq. (4) can be rewritten into:

$$f_j(a_0^r,...,a_n^r, T^r) = \alpha_j{\cdot}I_j - \alpha_j{\cdot}(a_0^r + ...+ a_i^r{\cdot}\lambda_j + ...a_n^r{\cdot}\lambda_j^n){\cdot}\frac{c_1}{\pi\lambda^5 e^{c_2/\lambda_j T}} \tag{5}$$

Where r represents iteration number. The question is turned into finding zero point for (5). The deviation can be achieved by substituting solutions into (5).

1) Partial derivative can be taken using equations:

$$\frac{\partial f_j}{\partial a_i} \approx \frac{f_j(a_0^r, ..., a_i^r + \delta a_i, ..., a_n^r, T^r) - f_j(a_0^r, ..., a_i^r, ..., a_n^r, T^r)}{\delta a_i}$$
$$\frac{\partial f_j}{\partial T} \approx \frac{f_j(a_0^r, ..., a_i^r, ..., a_n^r, T^r + \delta T) - f_j(a_0^r, ..., a_i^r, ..., a_n^r, T^r)}{\delta T} \tag{6}$$

Where δ represents slight deviation superposed on the point to get partial derivative.

1) Correction value

According to the deviation and partial derivative, correction value in rth step can be achieved using the relationship expressed as:
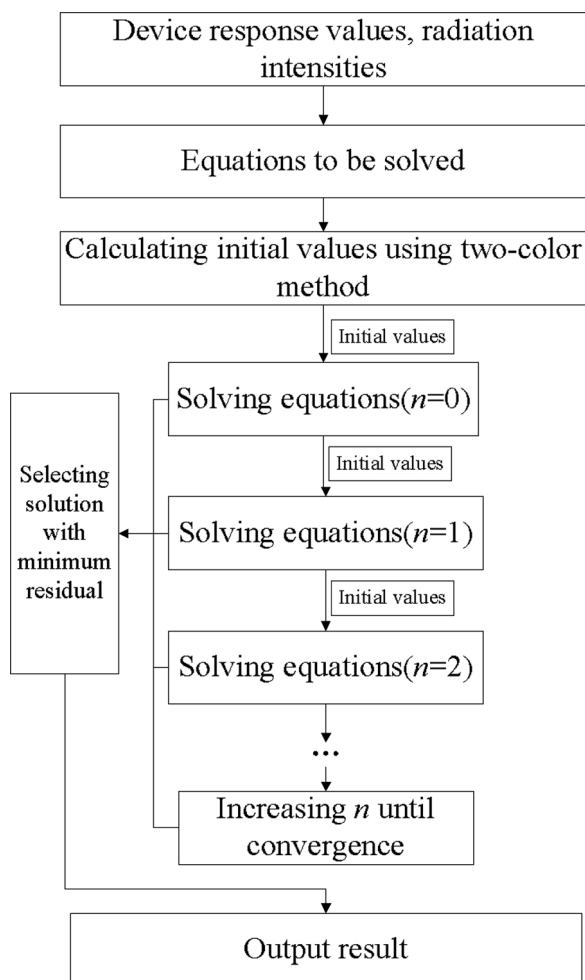
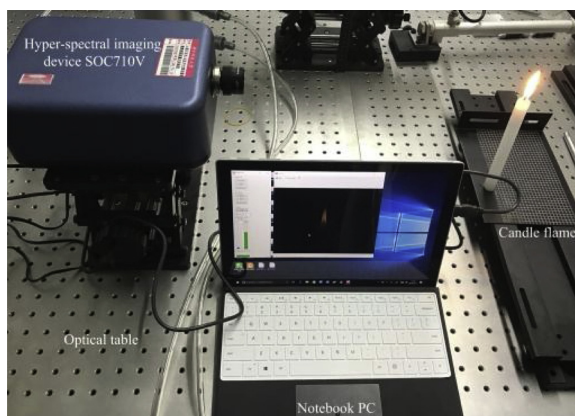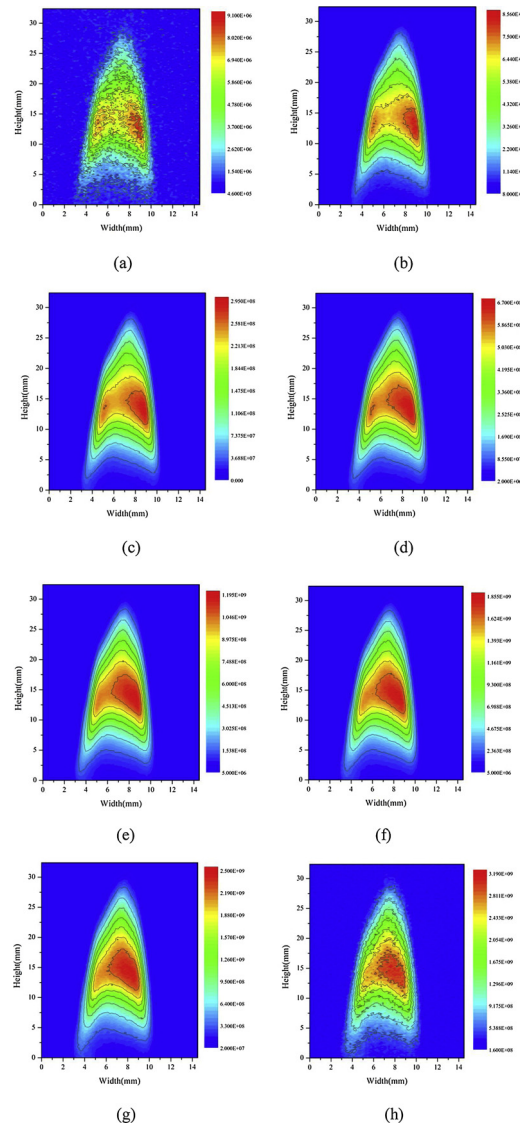**Fig. 1.** Photograph of calculation process.

Fig. 2. Photograph of experimental set-up.

Fig. 3. Hyperspectral images of the flame radiation intensity (Wm^{-3} sr^{-1}). Including 8 sheets of images from various available wavelengths, specially (a) $\lambda_1 = 447.66$ nm, (b) $\lambda_2 = 528.84$ nm, (c) $\lambda_3 = 611.10$ nm, (d) $\lambda_4 = 694.44$ nm, (e) $\lambda_5 = 778.86$ nm, (f) $\lambda_6 = 864.35$ nm, (g) $\lambda_7 = 950.93$ nm, (h) $\lambda_8 = 1038.60$ nm.

$$
\begin{bmatrix} f_1^r \\ \cdot \\ f_j^r \\ \cdot \\ f_m^r \end{bmatrix} = \begin{bmatrix} \frac{\partial f_1}{\partial a_0}^r & \cdot & \frac{\partial f_1}{\partial a_n}^r & \frac{\partial f_1}{\partial T}^r \\ \cdot & \cdot & \cdot & \cdot \\ \frac{\partial f_j}{\partial a_0}^r & \cdot & \frac{\partial f_j}{\partial a_n}^r & \frac{\partial f_j}{\partial T}^r \\ \cdot & \cdot & \cdot & \cdot \\ \frac{\partial f_m}{\partial a_0}^r & \cdot & \frac{\partial f_m}{\partial a_n}^r & \frac{\partial f_m}{\partial T}^r \end{bmatrix} \cdot \begin{bmatrix} \Delta a_0^r \\ \cdot \\ \Delta a_n^r \\ \Delta T^r \end{bmatrix}
$$

$$(7)$$

Where Δ represents the correction value. Eq. (7) is a system of linear equations. Therefore, it can be solved using least square method.
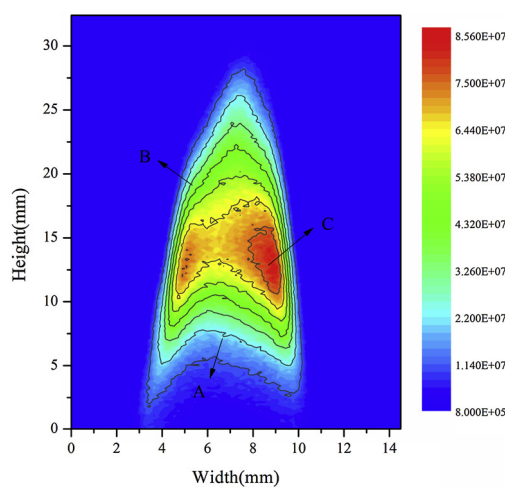
1) Solution updating

After achieving correction value for the solution of last iteration or initial value, solution for this iteration can be calculated using:
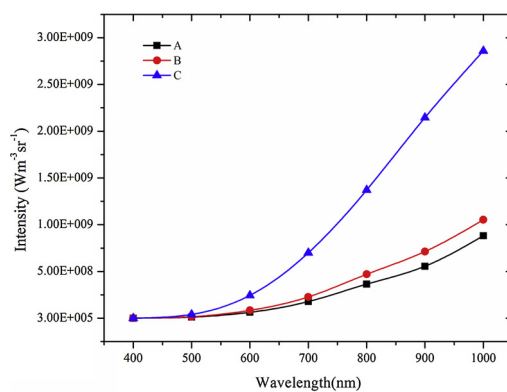
$$[a_0^{r+1}, \ldots, a_n^{r+1}, T^{r+1}] = [a_0^r, \ldots, a_1^r, T^r] - [\Delta a_0^r, \ldots, \Delta a_n^r, \Delta T^r] \qquad (8)$$

Fig. 4. (a) candle flame image measured by the hyperspectral imaging technology (b) One sheet of hyperspectral images of the flame radiation intensity ($Wm^{-3} sr^{-1}$) $\lambda = 529$ nm; (c) The flame radiation intensity varying with wavelength for A,B,C ($Wm^{-3} sr^{-1}$).
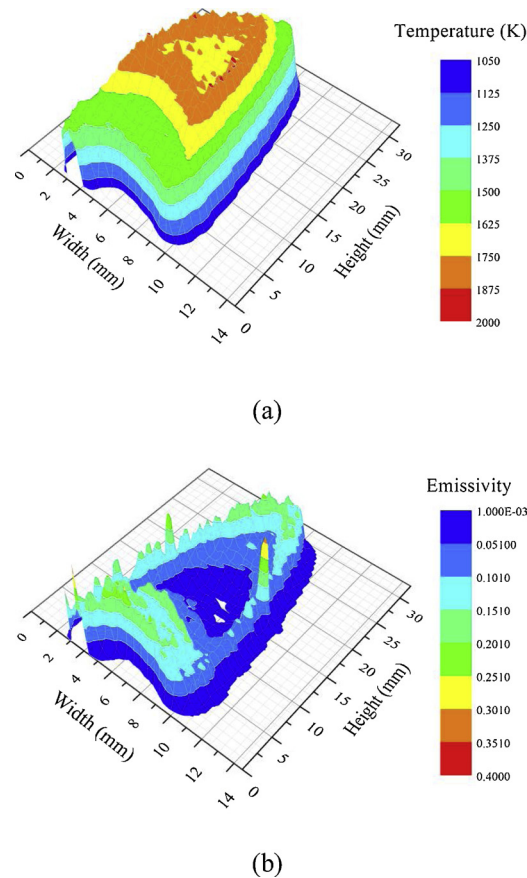
(a)

(b)

Fig. 5. (a) Image of radiation temperature and (b) 528.84 nm emissivity distribution.

3. Results and discussion

Radiation images were taken with a hyper-spectral imaging system(Type: SOC710-VP; Surface Optics Corporation, San Diego, CA, USA). The camera can take images of flame and create 128 sheets of images with 696 (h) × 520 (v) pixels. Fig. 2 is the experimental set-up, which includes an ordinary candle, PC, optical table and hyper-spectral imaging device. Spectral range is from 372.53 nm to 1038.60 nm. Resolution is 4.68 nm and band number is 128. The speed of hyper-spectral imaging system is 30 spatial lines per second. In the experiments presented here only steady laminar candle flames were recorded. When steady state burning was achieved, the hyperspectral images were taken of the flame. The experimental atmosphere temperature is 298 K, and the pressure is 1 atm. The diameter of the candle is 11.2 mm and the main components of the candle are dodecane and octadecane.

As shown in Fig. 3, the hyperspectral images contain spatial and spectral information, which can be used to analyze the spatial and spectral distribution of the flame radiation characteristics. We take the image data at a height of 32.4 mm and width of 14.5 mm as the data processing region. The results of the analysis shown in Fig. 3 reveal that the spectral radiation intensity increases from the outside to the inside in the candle flame. Also, at the same spatial location, the intensity increases as the wavelength increases.

Fig. 4 is one sheet of hyper-spectral images of the flame radiation intensity. Fig. 4(a) is the candle flame image. Fig. 4(b) is the image of the flame radiation intensity whose wavelength is 529 nm. This figure reveal that the spectral radiation intensity increases from the outside to the inside in the candle flame. Also, we can get the changing trend of the same spatial location A, B, C when the wavelength increases. A represents the flame bottom region at the width of 7 mm for the height of 6 mm. B represents the flame upper region at the width of 5 mm for the height of 18 mm. C represents the flame middle region at the width of 9 mm for the height of 12.5 mm. As is shown in Fig. 4(c), the intensity increases as the wavelength increases.

The estimated radiation temperature distribution is shown in Fig. 5. The results in Fig. 5(a) reveal that the highest temperature, which is about 1980 K, occurs near the flame border. Thomsen et al. [13] measured the peak temperature of the candle flame between 2000 and 2200 K, which proves that the result in Fig. 5 is reasonable. The highest temperature location indicates the most intense combustion reaction, which is controlled by the amount of air and fuel. For the position near the wick, the amount of air transmitted by the diffusion is insufficient. For the position far from the wick, the amount of fuel provided by the diffusion is the limiting factor. Thus, the most intense reaction occurs in the middle of these zones, near the flame border. Also, it can be seen that the trend of the change of the temperature was opposite to that of the emissivity.

The distribution of wavelength-dependent emissivity from various available wavelengths is shown in Fig. 6. At the same position,
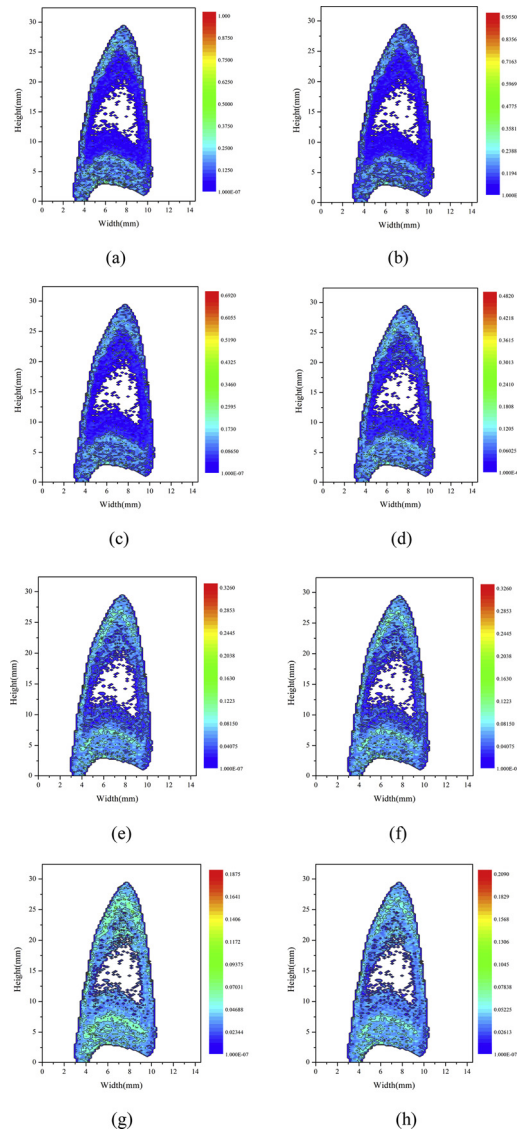
Fig. 6. Wavelength-dependent emissivity distribution of flame. Including 8 images of emissivities from various available wavelengths : $\lambda_1 = 447.66\,nm$, $\lambda_2 = 528.84\,nm$, $\lambda_3 = 611.10\,nm$, $\lambda_4 = 694.44\,nm$, $\lambda_5 = 778.86\,nm$, $\lambda_6 = 864.35\,nm$, $\lambda_7 = 950.93\,nm$, $\lambda_8 = 1038.60\,nm$.

the emissivity decreases with the increase of wavelength. Moreover, the highest emissivity occurs in the zone near the flame border, while the emissivity is very low near the flame center because of the wick. The existence of the wick leads to the failure of the model to calculate emissivities.

The calculated radiative temperature at the height of 7.16 mm, 17.9 mm and 25.06 mm are given in Fig. 7(a). Where, the trends can be shown more clearly distinguished, thus allowing to draw definite conclusion. For a height of 7.16 mm or 25.06 mm, there is a marked drop in temperature at the center of the flame because of the wick, while for a height of 17.9 mm, the temperature is the highest at the center of the flame because there is no wick influence. The emissivity distribution at 550 nm wavelength is shown in Fig. 7(b). For a height of 7.16 mm, the peak emissivity is 0.29 at a width of 7 mm, while for a height of 25.06 mm, the peak emissivity is 0.24 at a width of 6 mm. In contrast, for a height of 17.9 mm, the peak emissivity is 0.225 at a width of 4.8 mm, but the emissivity is complex at the center of the flame because of the influence of the wick and soot.

The spectral distribution of emissivity for three characteristic points at the height of 7.16 mm, 17.9 mm and 25.06 mm is shown in Fig. 8. It can be seen that there is an approximately inverse relationship between the emissivity and the wavelength, consistent with results obtained by Rayleigh approximation [22]. The reason is that the emissivity is determined by the absorption coefficient along the line of sight. And the absorption coefficient is the result of a cumulative effect. In other words, the emissivity is determined by the sum of the average line-of-sight absorption coefficient and the path length, or optical thickness.

The two-color method is a common method to calculate radiation temperature. If the emissivity of an object is considered to be
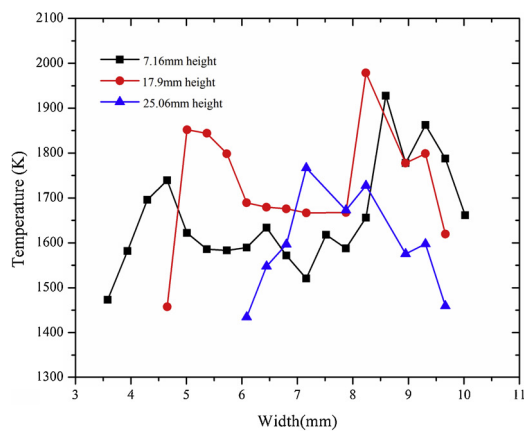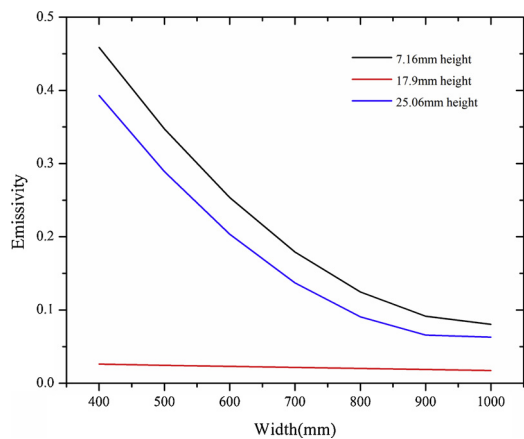
(a)
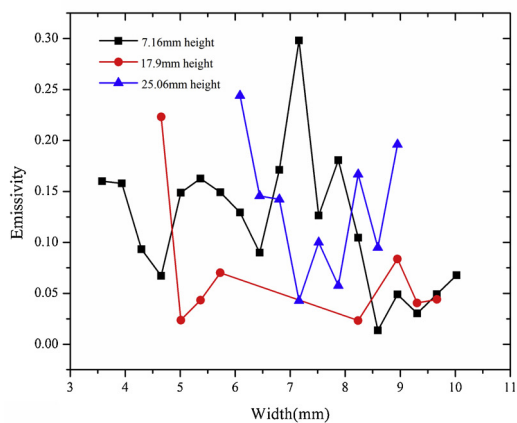
(b)

Fig. 7. Distribution of the estimated radiation temperature and the emissivities at 550 nm wavelength for the height of 7.16, 17.9 and 25.06 mm. (a) Distribution of the estimated radiation temperature for the three representative heights. (b)Emissivity distribution at 550 nm wavelength for the three representative heights.

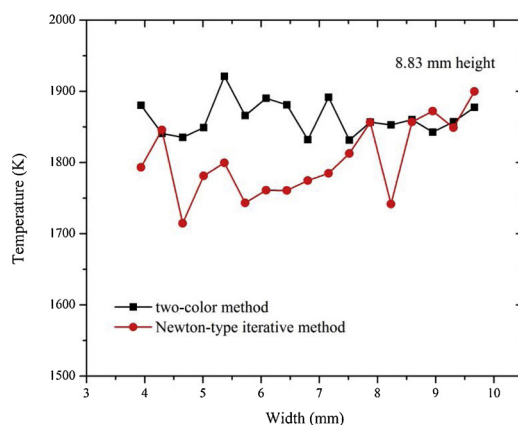**Fig. 8.** Emissivity distribution as a function of the wavelength at height of 7.16,17.9 and 25.06 mm.

Fig. 9. Comparison between the temperature calculated by the Newton-type iterative method and the two-color method at the height of 8.83 mm.

the same at two wavelengths, that is, assuming that the object is a gray, the radiative temperature can be calculated by the ratio of radiation intensity at two wavelengths. The comparisons of temperature at the height of 17.9 mm obtained by the Newton-type iterative method and the two-color method are shown in Fig. 9. It can be seen that the maximum relative error 6.84% appears at the width of 6.08 mm and the minimum relative error 0.002% appears at the width of 7.87 mm.

4. Conclusions

An experiment using a hyperspectral imaging camera is conducted to study a candle flame. The main conclusions are:

(1) The radiation characteristics of the candle flame different from a gray-body radiation, and the emissivity changed with the wavelength.
(2) The emissivity decreases as the wavelength increases, there is an approximately inverse relationship between the emissivity and the wavelength.
(3) The maximum emissivity (not including the flame center) is about 0.4 when wavelength is 400 nm.
(4) The highest temperature, which is about 1980 K, occurs near the flame border, indicating the location of the most vigorous reaction.

Acknowledgements

References

[1] F.B. Carleton, F.J. Weinberg, Electric field-induced flame convection in the absence of gravity, Nature 330 (1987) 635–636.
[2] T. Maxworthy, The flickering candle: transition to a global mode in a thermal plume, J. Fluid Mech. 390 (1999) 297–323.
[3] R.oss HD, S.otos RG, T.ien JS, Observations of candle flames under various atmospheres in microgravity, Combust. Sci. Technol. 75 (1991) 155–160.
[4] D.L. Dietrich, H.D. Ross, Y. Shu, P. Chang, J.S. T'Ien, Candle flames in non-buoyant atmospheres, Combust. Sci. Technol. 156 (2000) 1–24.
[5] K.M. Allan, J.R. Kaminski, J.C. Bertrand, J. Head, P.B. Sunderland, Laminar smoke points of wax candles, Combust. Sci. Technol. 181 (2009) 800–811.
[6] A. Hamins, M. Bundy, S.E. Dillon, Characterization of candle flames, Brief. Funct. Genomics 15 (2005) 265–285.
[7] P.B. Sunderland, J.G. Quintiere, G.A. Tabaka, D. Lian, C.W. Chiu, Analysis and measurement of candle flame shapes, Proc. Combust. Inst. 33 (2011) 2489–2496.
[8] J.S. T'Ien, Modelling of candle burning with a self-trimmed wick, Combust. Theory Model. 12 (2008) 367–388.
[9] J. Ma, Y. Sun, B. Li, Spectral collocation method for transient thermal analysis of coupled conductive, convective and radiative heat transfer in the moving plate with temperature dependent properties and heat generation, Int. J. Heat Mass Transf. 114 (2017) 469–482.
[10] W. Fuqiang, W. Hao, G. Dayang, C. Ziming, M. Lanxin, Radiative transfer analysis of semitransparent medium with particles having non-uniform size distribution by differential-integration method, Int. J. Heat Mass Transf. 130 (2019) 342–355.
[11] S. Zheng, Y. Yang, H. Zhou, The effect of different HITRAN databases on the accuracy of the SNB and SNBCK calculations, Int. J. Heat Mass Transf. 129 (2019) 1232–1241.
[12] A. Patel, Temperature measurement of a candle flame using a CCD camera, Interim Report, (2008).
[13] M.C. Thomsen, A. Fuentes, R. Demarco, C. Volkwein, J.L. Consalvi, P. Reszka, Soot measurements in candle flames, Exp. Therm. Fluid Sci. 82 (2017) 116–123.
[14] C. Lou, C. Chen, Y.P. Sun, H.C. Zhou, Review of soot measurement in hydrocarbon-air flames, Sci. China Technol. Sci. 53 (2010) 2129–2141.
[15] L. Yang, Z.H. Wang, Y.Q. Zhu, Z.S. Li, J.H. Zhou, Z.Y. Huang, K.F. Cen, Premixed jet flame characteristics of syngas using OH planar laser induced fluorescence, Chinese Sci. Bull. 56 (2011) 2862–2868.
[16] G. Zhe, C. Lou, Z.D. Liu, H.C. Zhou, The impact of combustion characteristics and flame structure on soot formation in oxy-enhanced and oxy-fuel diffusion flames, Sci. China Technol. Sci. 56 (2013) 1618–1628.
[17] S. Wagner, B.T. Fisher, J.W. Fleming, V. Ebert, TDLAS-based in situ measurement of absolute acetylene concentrations in laminar 2D diffusion flames, Proc. Combust. Inst. 32 (2009) 839–846.

[18] C. Liu, L. Xu, Z. Cao, H. Mccann, Reconstruction of axisymmetric temperature and gas concentration distributions by combining fan-beam TDLAS With onion-peeling deconvolution, IEEE Trans. Instrum. Meas. 63 (2014) 3067–3075.

[19] Y. Du, Z. Peng, Y. Ding, High-accuracy sinewave-scanned direct absorption spectroscopy, Opt. Express 26 (2018) 29550–29560.

[20] F. Liu, K.A. Thomson, G.J. Smallwood, Effects of soot absorption and scattering on LII intensities in laminar coflow diffusion flames, J. Quant. Spectrosc. Radiat. Transf. 109 (2008) 337–348.

[21] Q.X. Huang, F. Wang, D. Liu, Z.Y. Ma, J.H. Yan, Y. Chi, K.F. Cen, Reconstruction of soot temperature and volume fraction profiles of an asymmetric flame using stereoscopic tomography, Combust. Flame 156 (2009) 565–573.

[22] D.R. Snelling, K.A. Thomson, G.J. Smallwood, L. Oslash, Guacute, E.J. lder, R.A. Weckman, Fraser, Spectrally resolved measurement of flame radiation to determine soot temperature and concentration, Aiaa J. 40 (2002) 1789–1795.

[23] S.D. Iuliis, M. Barbini, S. Benecchi, F. Cignoli, G. Zizak, Determination of the soot volume fraction in an ethylene diffusion flame by multiwavelength analysis of soot radiation, Combust. Flame 115 (1998) 253–261.

[24] H. Liu, S. Zheng, H. Zhou, C. Qi, Measurement of distributions of temperature and wavelength-dependent emissivity of a laminar diffusion flame using hyper-spectral imaging technique, Meas. Sci. Technol. 27 (2016) 025201.

[25] H. Liu, S. Zheng, H. Zhou, Measurement of soot temperature and volume fraction of axisymmetric ethylene laminar flames using hyperspectral tomography, IEEE Trans. Instrum. Meas. 66 (2017) 315–324.

[26] P.M. Mehl, Y.R. Chen, M.S. Kim, D.E. Chan, Development of hyperspectral imaging technique for the detection of apple surface defects and contaminations, J. Food Eng. 61 (2004) 67–81.

[27] A.A. Gowen, C.P. O'Donnell, P.J. Cullen, G. Downey, J.M. Frias, Hyperspectral imaging – an emerging process analytical tool for food quality and safety control, Trends Food Sci. Technol. 18 (2007) 590–598.

[28] W. Yan, H. Zhou, Z. Jiang, C. Lou, X. Zhang, D. Chen, Experiments on measurement of temperature and emissivity of municipal solid waste (MSW) combustion by spectral analysis and image processing in visible spectrum, Energy Fuels 27 (2013) 6754–6762.

[29] J.L. Gardner, A Six-Wavelength Radiation Pyrometer, High Temp High Pressures, (1981).